

# Evidence for an outflow from the Seyfert galaxy NGC 4051

P.E. Christopoulou,<sup>1</sup> A.J. Holloway,<sup>2</sup> W. Steffen,<sup>2</sup> C.G. Mundell,<sup>3</sup>  
 A.H.C. Thean,<sup>3</sup> C.D. Goudis,<sup>1</sup> J. Meaburn,<sup>2</sup> and A. Pedlar<sup>3</sup>

<sup>1</sup>*Department of Physics, University of Patras, Patras 26500, Greece*

<sup>2</sup>*Department of Physics and Astronomy, University of Manchester, Schuster Laboratory, Oxford Road, Manchester M13 9PL, UK*

<sup>3</sup>*Nuffield Radio Astronomy Laboratories, University of Manchester, Jodrell Bank, Macclesfield, Cheshire SK11 9DL, UK*

Accepted for publication August 1996

## ABSTRACT

New observations using narrow band imaging, long-slit spectroscopy and MERLIN observations of the nuclear region of the Seyfert galaxy NGC 4051 have been made. An edge brightened, triangular region of ionized gas extending 420 pc from the centre of the galaxy has been detected. Long-slit spectra of this ionised gas, taken at 1.5'' from the core, show the [O III] 5007-Å emission line to consist of two velocity components, both blue-shifted from the systemic radial velocity, with velocity widths of 140 kms<sup>-1</sup> and separated by 120 kms<sup>-1</sup>. This region is co-spatial with weak extended radio emission and is suggestive of a centrally driven outflow. The [O III] 5007-Å line spectrum and image of this region have been modelled as an outflowing conical structure at 50° to the line of sight with a half opening angle of 23°.

In addition to the extended structure, high resolution MERLIN observations of the 18-cm nuclear radio emission reveal a compact (1'') radio triple source in PA 73°. This source is coincident with the HST-imaged emission line structure. These high resolution observations are consistent with a more compact origin of activity (i.e. a Seyfert nucleus) than a starburst region.

**Key words:** galaxies: active - galaxies: jets - galaxies: kinematics and dynamics - galaxies: Seyfert - galaxies: individual: NGC 4051

## 1 INTRODUCTION

Anisotropic emission in Active Galactic Nuclei (AGN), and, in particular, Seyfert galaxies, has become fairly well established although the mechanisms of fuelling and collimating ejecta remain problematic. In Seyfert galaxies, the closest and a very common type of AGN, both the radio and optical emission are often observed to be emitted in a collimated fashion.

Seyfert galaxies are classified, according to the width of their emission lines (Khachikian & Weedman 1971), into two main types: Type 1's (with broad permitted and narrow forbidden lines) and Type 2's (with narrow permitted and forbidden lines). The discovery of a hidden Broad Line Region (BLR) (Antonucci & Miller 1985) and non-stellar continuum in the polarised flux spectrum of the Seyfert type 2 galaxy, NGC 1068, led to the present day Unified Schemes in which the different observed properties of Seyfert types 1 and 2 may be accounted for by viewing angle. Antonucci & Miller (1985) suggested that the nucleus in Seyfert type 2's are obscured from direct view by an optically and geometrically thick disk or torus but that the hidden BLR can be seen

when nuclear radiation is scattered, by electrons above and below the poles of the torus, into the observer's line of sight. This obscuring torus would also give rise to an anisotropic nuclear radiation field.

Direct optical evidence for this anisotropic radiation field was provided by the discovery of the Extended Narrow Line Region (ENLR) (Unger et al. 1987). The physical and kinematic properties of the ENLR (e.g., FWHM  $\leq$  45 km s<sup>-1</sup>, [O III] 5007-Å/H $\beta$   $\sim$  10) implied that it is ambient galactic gas photoionized by the nuclear UV continuum radiation. This was confirmed by the discovery of a number of extended emission line regions (Meaburn, Whitehead & Pedlar 1989, Pogge 1989, Pedlar et al. 1989, Tadhunter & Tsvetanov 1989, Unger et al. 1992, Wilson & Tsvetanov 1994), ranging in size from  $\sim$ 70 pc to  $\sim$ 20 kpc (Wilson & Tsvetanov 1994), consistent with ionisation by a UV radiation cone.

Until recently the relatively poor angular resolutions of ground based optical measurements and small linear extents of the NLRs resulted in limited evidence for NLR 'cones' in Seyferts. However, the discovery of NLR 'cones' in NGC

4151 (Evans et al. 1993, Boksenberg et al. 1995), NGC 3281 (Storchi-Bergman, Wilson & Baldwin 1992), and NGC 3227 (Mundell et al. 1995) suggests that this phenomenon may be more widespread.

It should be noted that an ENLR is physically distinct from a Narrow Line Region (NLR), which has broader emission lines (several hundred  $\text{kms}^{-1}$ ), is more directly affected by the active nucleus and may involve different physical processes to the ENLR. In some Seyferts, the optical emission may be a signature of the physical interaction between the radio ejecta and the surrounding medium (e.g., Whittle et al. 1986, Pedlar et al. 1989) as in the model proposed by Taylor, Dyson & Axon (1992). Therefore, any detection of emission line regions, consistent with a cone of ionising UV, should be considered carefully together with kinematic information to determine its true nature.

Although Seyferts are radio ‘quiet’, they are not radio silent and many Seyferts exhibit radio anisotropy in the form of highly collimated radio jets (e.g., Wilson & Ulvestad 1987, Pedlar et al. 1993, Kukula et al. 1995). Although radio jets have typical opening angles of only a few degrees, compared with ionisation cones of up to  $\sim 100$  degrees, there are good alignments between ENLRs and radio jet axes in a number of Seyferts (Wilson & Tsvetanov 1994). The alignments suggest that the radio ejecta and UV photons are collimated by the same, or co-planar, structures with no significant relative precession (Tsvetanov, Kriss & Ford 1994). In those Seyferts which exhibit misaligned radio jets and ionisation wedges, it may be that the UV cone of radiation (which is assumed to share the same collimation direction as the radio jet) points partly out of the galactic disk. The UV cone then grazes the neutral galactic disk producing an ionised wedge (in the disk) that is misaligned from the radio jet due to projection effects on the sky (Pedlar et al. 1993, Robinson et al. 1994).

Not all Seyferts have well-collimated radio jets and a distinction should be made between those with jets and those with more diffuse, extended radio emission. Baum et al. (1993) find large-scale, diffuse, sometimes ‘bubble-like’, radio emission from 12 Seyferts, including NGC 4051. They note that the large-scale, ‘extra-nuclear’ radio emission is randomly oriented with respect to any small-scale nuclear radio source axis and tends to align with the minor axis of the host galaxy. They attribute this diffuse component of the radio emission to radio-emitting superwind that has been produced and swept out along the galaxy’s minor axis by a circum-nuclear starburst.

NGC 4051 has been the subject of a number of studies in the past and in Table 1 we list the morphological parameters from previous observations. At radio wavelengths structure has been seen on a number of scales. The VLA observations by Ulvestad & Wilson (1984) at 6cm detect the  $0.4''$  double source at  $\text{PA } 78^\circ \pm 6^\circ$ , with more extended emission ( $\sim 2''$ ) to the southwest in their 20cm map. On a much larger scale, Baum et al. (1993) detect 3 regions of 6cm radio emission: a ‘banana-shaped’ nuclear region ( $15''$  in extent) along  $\text{PA } 32^\circ$  (the minor axis of the galaxy), an extra-nuclear diffuse radio emission region from the spiral arms and large-scale radio emission from the entire galaxy disk. The 8.4 GHz VLA C-array maps from Kukula et al. (1995) shows a bright elongated source at  $\text{PA } 37^\circ$  with a total extent of  $15''$ .

The [O III] 5007-Å image of Haniff, Wilson & Ward

(1988) contains a compact emission line region of overall extent  $3''$  at  $\text{PA } 81^\circ \pm 5^\circ$ , which suggests that the orientation and extent of the high excitation emission line gas are essentially the same as those of the nuclear radio continuum emission. The main characteristic of the narrow line profiles of NGC 4051 present in all the forbidden lines, is the strong blue wing extending to velocities of  $\sim 800 \text{ kms}^{-1}$  with substructures especially evident in the profiles of [O III] 4959, 5007-Å (Veilleux 1991).

In the present paper we describe new optical and radio observations of the Seyfert galaxy NGC 4051. We adopt a distance of 9.7 Mpc, using a value of  $H_0 = 75 \text{ kms}^{-1} \text{ Mpc}^{-1}$  and its redshift of  $726 \text{ kms}^{-1}$  (Ulvestad & Wilson 1984). One arcsecond therefore equals 47 pc at the galaxy.

## 2 OBSERVATIONS AND RESULTS

### 2.1 MES [O III] 5007-Å narrow band imaging

Narrow band imaging in the light of the [O III] 5007-Å emission line was carried out on 1993 June 11 using the Manchester Echelle Spectrograph (MES - Meaburn et al. 1984) in its imaging mode, combined with the f/15 Cassegrain focus of the 2.5m Isaac Newton Telescope. An EEV CCD (1280x1180 pixels) detector was used to provide a binned 2x2 array of 640x590 pixels which, at the f/15 focus, provided a pixel scale of  $0.255''/\text{pixel}$ . During these observations the seeing was typically  $0.8''$ .

In the imaging mode a plane mirror is inserted to exclude the echelle grating and a clear aperture replaces the entrance slit. Four exposures, totalling 7600s, were made of the galaxy using a filter with a central wavelength of 5050Å and a bandwidth of 70Å to include the redshifted [O III] 5007-Å line. This filter also included the [O III] 4959-Å line but only at a level of  $\sim 8$  per cent of the total flux. To enable the continuum light to be subtracted from this image two images were taken using a V band (1000Å bandwidth) filter with a total exposure time of 300s.

The reduction of the data was carried out at the University of Manchester node of the UK STARLINK computer network using the FIGARO, CCDPACK and KAPPA packages. The images were processed in the usual way and then images through each filter were co-added to improve the signal-to-noise ratio. The images were aligned using the compact peak in emission from the nucleus of the galaxy. The [O III] 5007-Å image was then obtained by the subtraction of the V-band image from the [O III] 5007-Å + continuum image, being scaled, in the absence of any stars, so that the galactic disk disappeared in the final image.

The V-band image of the galaxy and continuum subtracted [O III] 5007-Å emission line image are displayed using a logarithmic scale and are shown in Fig. 1.

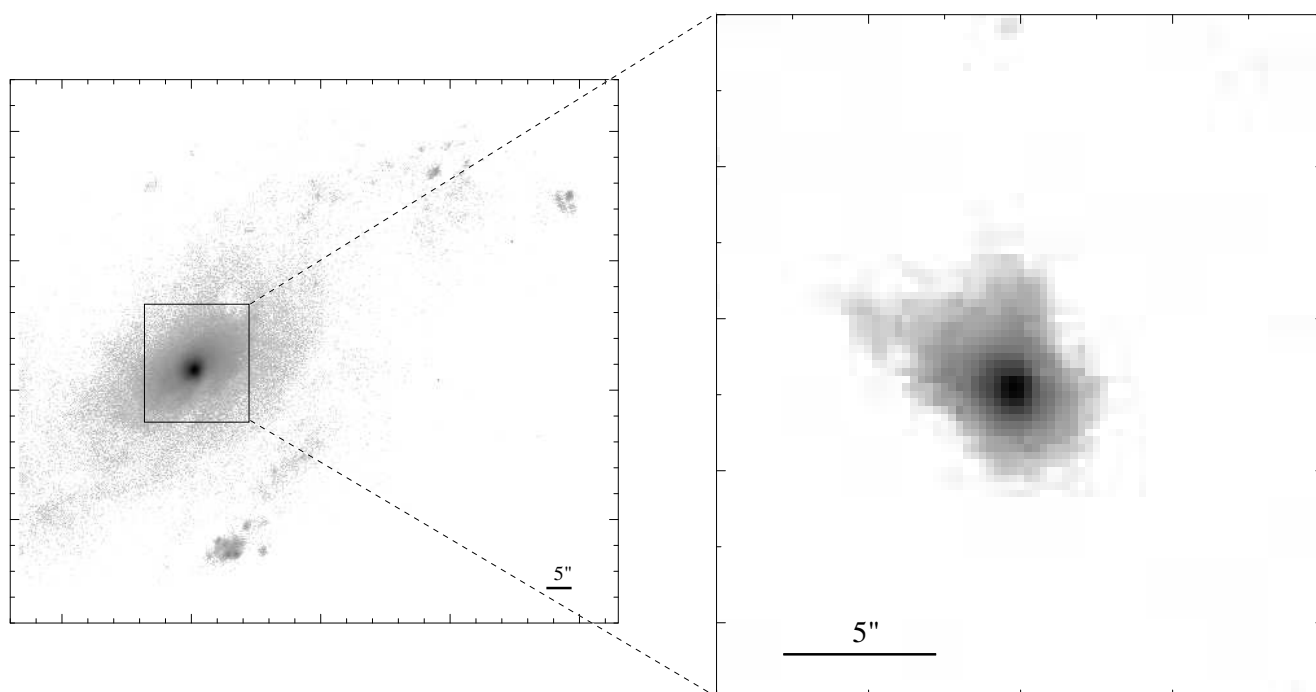
### 2.2 MES spectrometry

Spatially resolved spectral observations were made on 1993 June 11 using the same instrumental setup as described above. A single longslit was used with the 5050Å central wavelength filter and the redshifted [O III] 5007-Å line observed in the 113th echelle order. The integration time was 1800s, using the EEV CCD binned this time twice in the

**Table 1.** Morphological parameters for NGC 4051

Other name	UGC 07030	(Uppsala General Catalogue of Galaxies - UGC, Nilson 1973)
Seyfert type	Type 1	(Adams 1977)
	Type 1.5	(Dahari & De Robertis 1988)
Host galaxy	SB	(Catalogue of Principal Galaxies - CPG, Paturel et al. 1989)
	Sb or SBc	(UGC)
Magnitude (V)	12.9	(Veron-Cetty & Veron 1985)
Inclination	-40°	(Adams 1977)
Optical major axis PA	135°	(CPG, UGC)
Optical minor axis PA	32°	(CPG, UGC)
Heliocentric redshift	0.0023	(Dahari & De Robertis 1988)
$V_r^a$ (kms <sup>-1</sup> )	613	(Kukula et al. 1995)
$V_{\text{sys}}$ (kms <sup>-1</sup> )	726	(Ulvestad & Wilson 1984)
Optical flux density (mJy)	200	(Kukula et al. 1995)
$F([\text{O III}] 5007\text{-}\text{\AA})$ (10 <sup>-14</sup> ergs s <sup>-1</sup> cm <sup>-2</sup> )	52.1	(Dahari & De Robertis 1988)

<sup>a</sup> Heliocentric recession velocity.


**Figure 1.** MES INT V-band image (left) and [O III] 5007-Å image after continuum subtraction (right) of NGC 4051, displayed in negative using a logarithmic scale

spatial direction and by three times in the spectral dimension. This results in an array of 640 pixels along the slit length with a scale of 0.255''/pixel and 393 pixels in the wavelength axis with a spectral resolution of  $\sim 9$  kms<sup>-1</sup>. The slit of the spectrometer was rotated to a position angle of 27.5° to align it with that of the radio emission and centered on the nucleus of the galaxy. A slit width of 1.62'' on the sky was used and the seeing was typically 0.8''.

The data were reduced using the STARLINK FIGARO, CCDPACK, KAPPA and TWOSPEC packages. A tungsten lamp was used to flat-field the spectrum and a Th-Ar arc lamp was used to calibrate the wavelength to  $\pm 1$  kms<sup>-1</sup> accuracy. The rest wavelength for the [O III] 5007-Å line was taken as 5006.85Å.

The resulting position-velocity (pv) array is shown in

Fig. 2 with spectra averaged over 0.51'' regions along the slit and with fits from a two component Gaussian model.

### 2.3 Radio emission in NGC 4051 - 18cm MERLIN maps

NGC 4051 was observed by MERLIN in October 1993 at 1658MHz. An 18 hour observing run was carried out in phase referencing mode using the nearby calibrator 1200+468. The flux density was determined from observations of 3C286. The data were imaged using natural weighting (Fig. 3) resulting in an angular resolution of 0.35'' x 0.31''. The MERLIN radio maps show a 0.8'' triple source extended along PA 73°. The flux densities of the radio components are given in Table 2. In the naturally weighted image there is weak emission extending over 8'' in PA  $\sim 30^\circ$ , consistent with

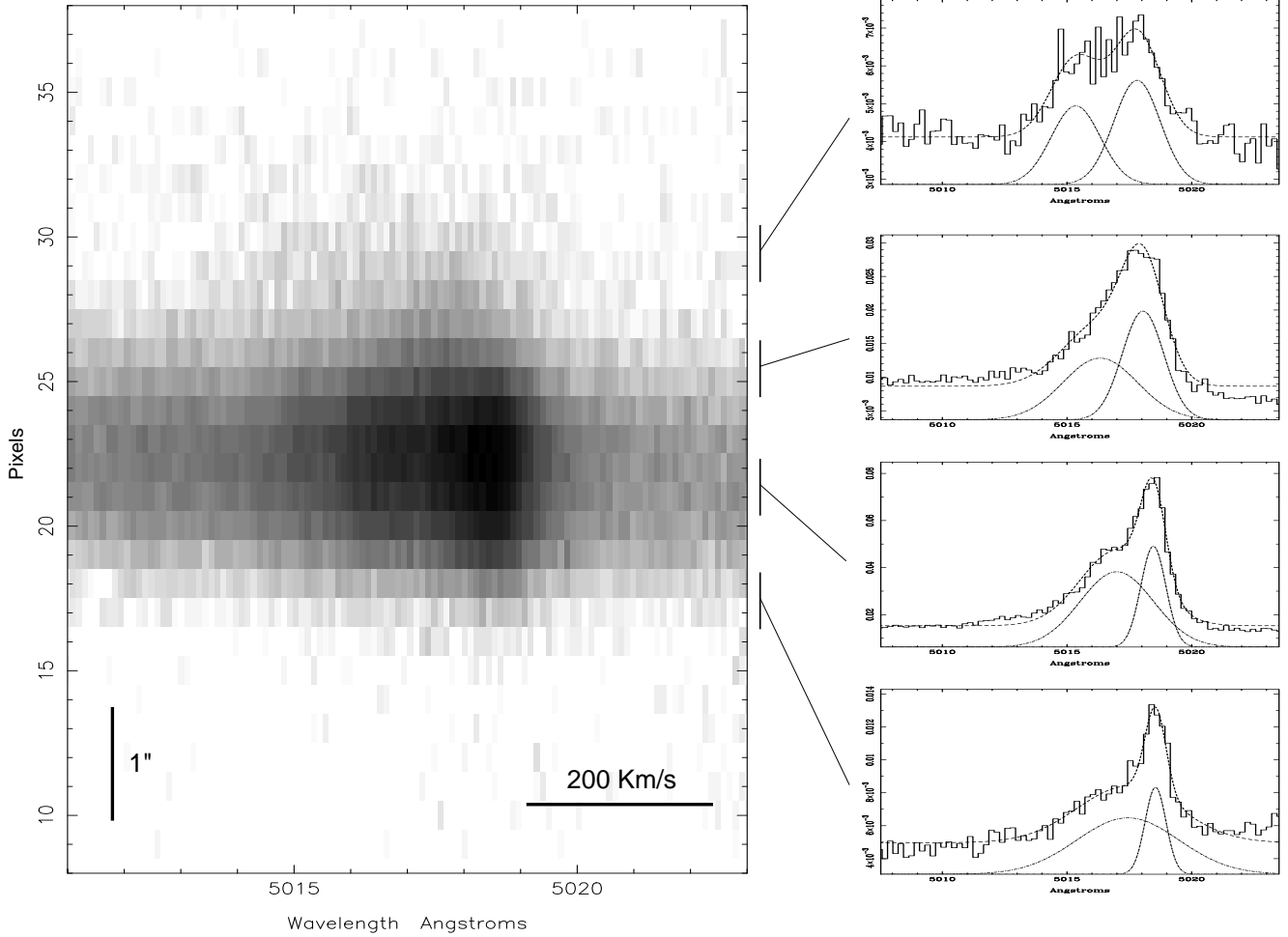


**Figure 2.** INT MES position-velocity map of [O III] 5007-Å emission along PA  $27.5^\circ$  displayed on a logarithmic scale. Spectra averaged over  $0.51''$  regions separated by  $1''$  are shown on the right with two-component Gaussian fits. North is to the top of the map.

lower resolution results reported by Baum et al. (1993) and Kukula et al. (1995).

#### 2.4 Archive HST data

For comparison with the MERLIN observations, Hubble Space Telescope (HST) images were obtained from the HST data archive. The observation was carried out using the F502N filter (including [O III] 5007-Å in the bandpass) with the Wide Field Planetary Camera I on 20th June 1991 (proposal no. 1036, H.C. Ford). This image has then been deconvolved using a model point spread function generated with the program TINY TIM, and applying the Lucy deconvolution routine within the IRAF package STSDAS. The image is shown in Fig. 4 with the MERLIN 1658 Mhz map overlaid as contours. A central  $0.6''$  linear feature is visible and more diffuse emission is seen out to a distance of  $3''$  in the HST image.

### 3 DISCUSSION

#### 3.1 The triangular emission line region

The [O III] 5007-Å MES image of NGC 4051 is shown in Fig. 5 with the 8 GHz VLA C-array map of Kukula et al. (1995) overlaid.

From the [O III] 5007-Å imaging (Fig. 1) we can clearly see the presence of a  $9''$  (420 kpc) ionised wedge in the centre. The wedge is bisected at a position angle of  $33^\circ$ , similar to that of the large scale radio axis (Fig. 5). The wedge is also therefore pointing along the minor axis of the galaxy (to within  $1^\circ$ ) as defined by the V-band image. The linear extent is similar to the radio emission seen in this direction, and the sharp edges of the [O III] 5007-Å wedge seem to follow the outline of the radio emission. The wedge is edge brightened and if its apex is assumed to be coincident with the nucleus of NGC 4051 then it has an apparent opening angle of  $55^\circ$ . No extended emission is detected to the southwest of the nucleus.

In the nuclear region of NGC 4051 (central  $0.5''$ ) the width (FWHM) of the [O III] 5007-Å line is  $240 \text{ km s}^{-1}$ , typical of NLR gas, though from the Gaussian fitting it does appear to have both a narrow and broad component. Spectra taken  $1.5''$  to the northeast of the nucleus (top plot, Fig.

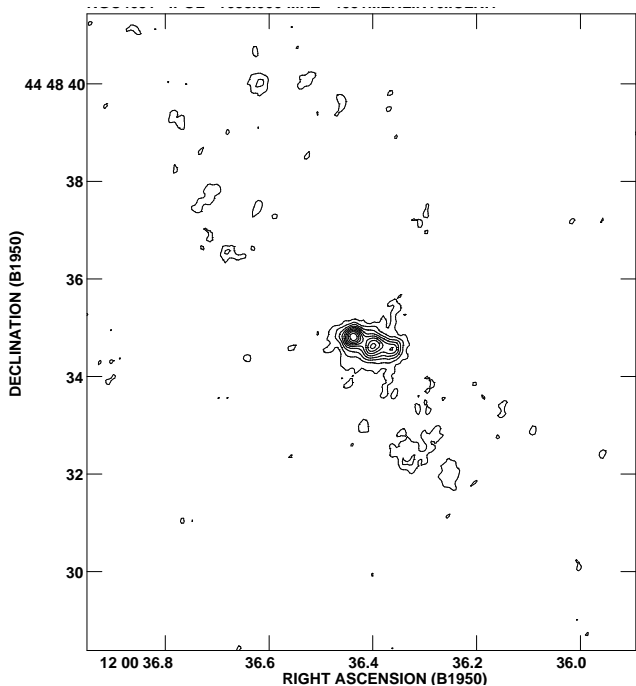


**Figure 3.** 18-cm MERLIN naturally weighted map of NGC 4051 with contours at  $14.52 \times (1, 2, 3, 4, 5, 6, 7, 8, 9)$  mJy

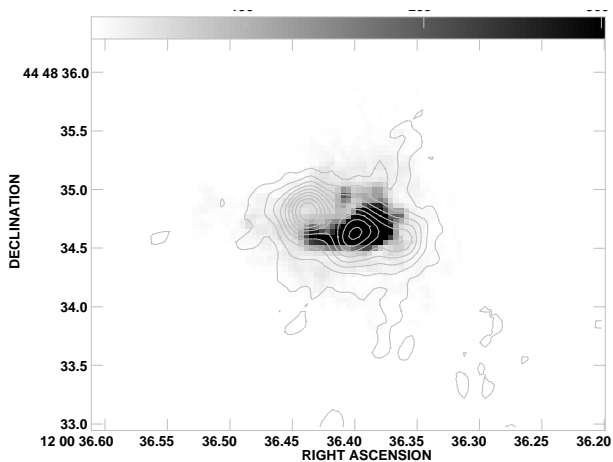


**Figure 4.** The HST F502N image is plotted as a greyscale with the MERLIN 18-cm map (Fig. 3) overlaid as contours.

2) show evidence of two equal components separated by  $\sim 120 \text{ km s}^{-1}$ , where both lines are  $\sim 140 \text{ km s}^{-1}$  wide and are blue-shifted by 80 and  $225 \text{ km s}^{-1}$  from the systemic radial velocity.

Similar linewidths and line-splitting are seen in the ionised wedges in NGC 3281 (Storchi-Bergman et al. 1992) and NGC 3227 (Mundell et al. 1995, Mundell 1995). Storchi-Bergman et al. (1992) propose a model in which outflow is taking place along an axis at a large angle to the plane of the galaxy. Unlike NGC 4051 and NGC 3227, in which both line components are blue-shifted, one of the components in NGC 3281 is red-shifted and the other blue-shifted. Therefore, they propose two possible geometries to explain their observed velocities; one where the cone axis is perpendicular to the plane of the galaxy and the other where the cone

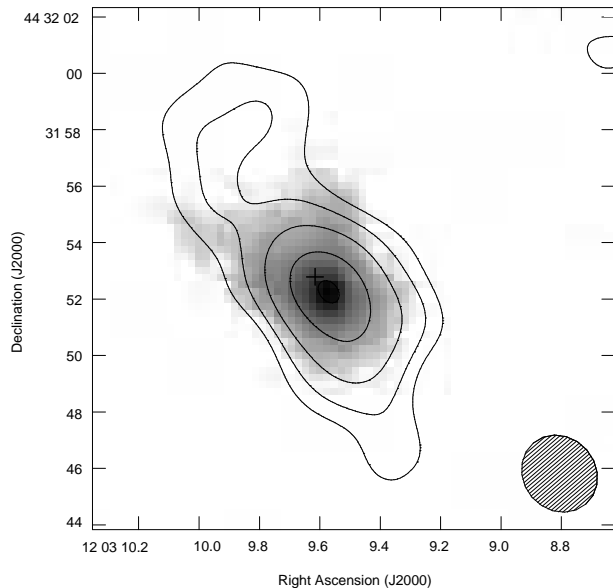


**Figure 5.** MES [O III] 5007-Å image (Fig. 1) overlaid with contours of the 8 GHz C-array VLA map of Kukula et al. (1995)

axis makes an angle of  $45^\circ$  with the disk. In their model, gas flows out within a conical envelope or on the surface of a hollow cone. The line-splitting is then attributed to the two components of velocity, along the line of sight, from the near and far sides of the cone.

We will now apply a similar model to NGC 4051 but, since both components are blue-shifted, the orientation of the outflow cone may be determined unambiguously.

### 3.2 Kinematic modelling of the extended emission line region

Our spectra reveal two velocity components, both blue shifted, which suggests that the axis of the emission cone is inclined towards the observer as shown in Fig. 6. Here the velocity along the sides of the cone is defined as  $v$ , with the inclination of the axis of the cone at  $\theta$  degrees to the line of sight and the cone having a half opening angle (for simplicity, hereafter ‘opening angle’) of  $\alpha$  degrees.

Assuming the cone to be circular in cross-section, the true opening angle of the cone,  $\alpha$ , is

$$\tan \alpha \approx \tan \alpha_{obs} \sin \theta, \quad (1)$$

where  $\alpha_{obs}$  is the observed opening angle of the cone.

If we assume the double velocity components present in the spectrum to be coming from opposite sides of the cone and the true velocity direction is along the sides of the cone, then the observed velocities  $v_1$  and  $v_2$  are defined by,

$$v_1 = v \cos(\theta - \alpha), \quad v_2 = v \cos(\theta + \alpha). \quad (2)$$

Using our values for the observed velocities of the Gaussian components in the spectrum  $v_1=225 \text{ km s}^{-1}$ ,  $v_2=80 \text{ km s}^{-1}$  and  $\alpha_{obs}=30^\circ$  we can solve equations (1) and (2) to obtain  $\theta = 48^\circ$ ,  $\alpha = 23^\circ$  and a velocity along the cone of  $v=245 \text{ km s}^{-1}$  (see Fig. 6). We use the [O III] 5007-Å line profiles as measured at more than  $1.5''$  from the nucleus in order to minimize contamination from the core region.

For simplicity, we used a Gaussian emissivity distribution for the wall of the cone (i.e. the emissivity drops smoothly away from the local radius of the wall). We assume that the emitting gas moves radially outwards from the vertex of the cone. We also assume that the emissivity along the jet axis drops with a Gaussian distribution (FWHM = 127 pc). Using the parameters derived from the spectrum and ground based image, this model yields a reasonably good approximation to the data (Figs. 7 and 8). However, the apparent opening angle in the simulated image and the exact shape of the spectrum both depend on the thickness of the wall of the cone.

Similarly, the width of the spectral line coming from each side of the cone is determined by the width of the wall. Note that in this model the side of the cone which is best aligned with the line of sight will have a smaller spectral width than the other. This effect can be seen in Fig. 8, where spectra are drawn with different wall thicknesses. Here a slit of width  $2.5''$  was set to be aligned with the cone axis, and a section between  $1.5''$  and  $2.1''$  from the core was used to produce this spectrum. The spectral resolution was  $9 \text{ km s}^{-1}$  and the spatial resolution was  $0.8''$ . A larger model slit width was used than in the observations to compensate for the image motion due to seeing, which was not taken into account explicitly. The solid line in Fig. 8 is for a FWHM equal to half the local radius of the cone, whereas the dashed line is for a FWHM twice as large. Because of the radial motion of the gas, thicker walls result in wider lines. This simulation can be compared with the spectrum of Fig. 2 taken  $1.5''$  from the core (top spectral plot). In Fig. 7 a model image of a wedge is shown with the observed MES [O III] 5007-Å image for comparison. The agreement is very good, considering the simplicity of this kinematic model. The main differences arise from not taking into account the central point source which produces a bright core at the vertex of the cone and a bright feature in the longslit spectrum. Hence, spectra produced from cuts through the model cone considerably closer to the core would not be expected to agree with the observed spectra. However, at  $1.5''$  (roughly 2 widths of the point spread function) we can expect a very reduced influence of the core emission, which affects mainly the height ratio of the spectral cone components. In our model, the height ratio is determined mainly by the emissivity variation along the axis of the cone.

Varying the parameters like the outflow velocity, the FWHM of the emissivity along the axis, the opening angle or the angle to the line of sight will produce results consistent with the observations with ranges of approximately plus or minus  $\Delta v = 30 \text{ km s}^{-1}$ ,  $\Delta \text{FWHM}_z = 20 \text{ pc}$ ,  $\Delta \alpha = 2 \text{ deg}$ , and  $\Delta \theta = 5 \text{ deg}$ , respectively. Based on this model, we suggest that in NGC 4051 the [O III] 5007-Å wedge represents a radial conical outflow with a half opening angle near  $23^\circ$  and a velocity of approximately  $250 \text{ km s}^{-1}$  at an angle to the line of sight of roughly  $50^\circ$ .

Note that in the two-component fit to the spectrum in Fig. 2, the component which is blue-shifted most gradually moves towards the systemic radial velocity and broadens as the core of the galaxy is approached. This does, of course, not happen in our model and may be due to a significant contribution of the redder line to the Gaussian fit of the bluer one. Unfortunately, the data quality does not allow a

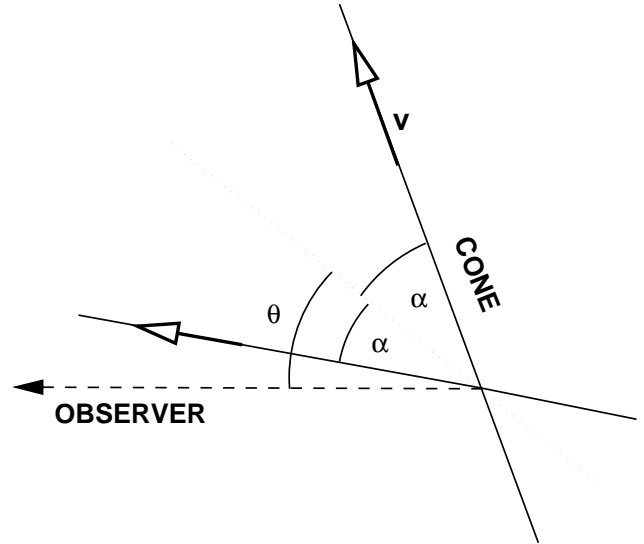


**Figure 6.** A schematic diagram illustrating the cone geometry.

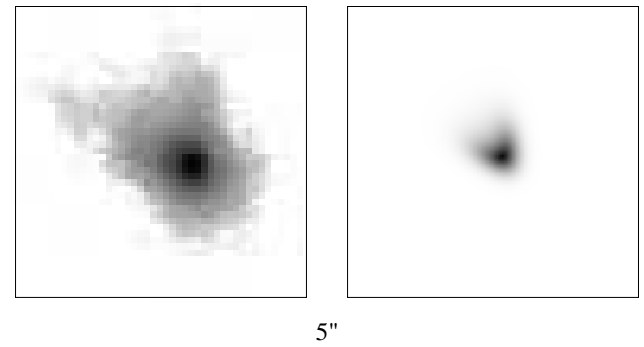


**Figure 7.** A comparison of the observed MES [O III] 5007-Å emission line wedge (left) with the image generated from the model (right).

well constrained three component fit to separate the core component from the cone components.

An alternative reason for this line shift may be that the cone does not have straight sides and may even change direction closer to the centre of the galaxy. This could also be combined with inhomogeneities in the cone wall. An observational indication of this is the position angle of the inner radio source, which is noticeably different from the outer one and the structure of the emission line gas in the HST-image (compare Fig. 1 and 4). However, these features are still consistent with the overall picture of an edge brightened, roughly conical outflow with a velocity around or in excess of  $200 \text{ km s}^{-1}$ .

Our conical model should be compared with an alternative physical model which is possible at least in principle. In this alternative model the observed wedge would actually be the inner edge of a plasma cloud which is expanding perpendicularly to its surface. A similar analysis to the one presented above, shows, however, that this is not consistent with the blue-shifted double-line, except if the ‘cone’ is on the far side of the galaxy. In this case, the observer’s line of sight would have to point inside the cone. Assuming a

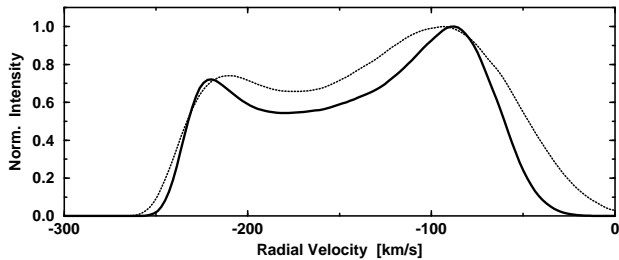


**Figure 8.** The model spectrum at  $1.5''$  from the nucleus. The dotted line is for a wall thickness comparable to the local cone radius, whereas the solid line corresponds to a wall thickness of half of the local cone radius. Compare this with the spectral plot at the top of Fig. 2.

**Table 2.** Radio parameters for NGC 4051

Component	Flux (mJy) 1.658 GHz	Flux (mJy) 8.439 GHz	Spectral Index (1.658/8.439)
East	1.6	0.05	2.1
Central	1.6	0.50	0.7
West	0.7	0.05	1.6

roughly uniform azimuthal emission distribution, this is not consistent with the observed edge brightening of the [O III] 5007-Å wedge. We therefore favour the scenario of a conical outflow with a vertex near the centre of the galaxy. Our simple outflow model does not provide a physical reason for the large scale ejection of the optically emitting gas. However, we speculate that it might be related to the collimated radio outflow or a large scale ‘superwind’ (Baum et al. 1993).

A trend seems to be emerging that an increasing number of cones detected in Seyfert galaxies are consistent with NLR rather than ENLR gas. The kinematics of the gas in these cones are more indicative of outflow rather than of anisotropic photoionisation of ambient galactic gas. The gas may be partially photoionized by the active nucleus but, if the radio ejecta are interacting with the optical gas, shock ionisation may also be present. The structure and kinematics, in particular line-splitting, of the [O III] 5007-Å emitting gas in the wedges in NGC 4051, NGC 3281, and NGC 3227 is consistent with conical outflow along the galactic density gradient.

### 3.3 The compact radio structure

Baum et al. (1993) have suggested that the extended radio emission seen in NGC 4051 is a consequence of outflow caused by a starburst driven ‘superwind’ which causes the optically emitting gas to flow out also. The ratio of  $60 \mu\text{m}$  to radio flux (Condon, Anderson & Broderick 1995) is also consistent with a starburst rather than a compact active nucleus. In general, starbursts are associated with diffuse radio emission, whereas Seyferts show collimated structures.

However, the high resolution maps made using MERLIN at 1658 Mhz (Fig. 3 reveal a compact ( $0.8''$ , 38 pc) triple source which favours collimated ejection in PA  $73^\circ$ . The 8GHz VLA A array image (Kukula et al. 1995) also shows weak structure consistent with the above triple, and by comparison with the 1658 Mhz image we can deduce the spectral indices of the components (see Table 2). It is clear

that the central component has the flattest spectral index of the triple, which would tentatively identify it as the AGN. The newly detected third component could therefore be part of a counter jet and the extended radio emission could represent a continuation of the central collimated flows somewhat analogous to Fanaroff-Riley 1 radio galaxy structures. However, in Seyfert galaxies the extended radio emission could be due to a debris of relativistic particles from frustrated jets flowing down the galactic density gradient similar to one of the models proposed for Mkn6 (Kukula et al. 1996). The fact that the HST structure (Fig. 4) bends towards PA  $\sim 30^\circ$  may also be evidence in favour of such a process.

The HST image (Fig. 4) shows a strong emission line structure of similar size to the radio triple with the western end of the optical feature being the brightest. Whilst the alignment of the HST image is subject to a pointing error of  $\sim 0.6''$  (Cox - private communication), this structure probably represents the base of the larger cone found in our ground based observations which engulfs the more extended weak radio emission. This is very similar to what has been found in Mkn 6 (Kukula et al. 1996).

## 4 CONCLUSIONS

We have found an edge-brightened extended emission line region exhibiting [O III] 5007-Å line splitting of up to  $\sim 120 \text{ km s}^{-1}$  at  $1.5''$  from the core. We suggest that this is due to a conical outflow with a flow velocity of approximately  $250 \text{ km s}^{-1}$  with its axis at roughly  $50^\circ$  to the line of sight. This engulfs the faint radio emission found on the same scale.

The MERLIN results show evidence for a subarcsecond radio triple source consistent with collimated ejection in PA  $73^\circ$  on a scale less than 40 pc. The three components are misaligned with respect to the large scale radio structure and optical emission line wedge, though there is evidence that the structures on these scales are linked.

Emission in the HST image seems to be the base of the emission line wedge found in our ground based image. Although the sub-structure of the HST and MERLIN images do not match each other, the overall extension of the brightest emission is similar in the emission line and the radio images and the compact radio emission again lies within the area covered by optical emission.

Our present observations cannot distinguish between whether or not the outflow is simply a continuation of the central collimated ejection associated with the Seyfert nucleus or possibly due to a starburst on a similar scale. Higher sensitivity, radio and HST imaging, together with dynamical studies are required to distinguish these possibilities.

## ACKNOWLEDGEMENTS

We thank M. Kukula for the postscript map of the 8 Ghz VLA C-array data. We acknowledge the support of the staff at the INT during these observations. AJH, WS, CGM, and AHCT acknowledge the receipt of a PPARC research studentship, associateship, fellowship and studentship respectively. PEC and CDG acknowledge support by the British Council during this work. We thank the anonymous referee for constructive comments.

## REFERENCES

- Adams T.F., 1977, *ApJS*, 33, 19
- Antonucci R.R.J., Miller J.S., 1985, *ApJ*, 297, 621
- Baum S.A., O'Dea C.P., Dallacassa D., De Bruyn A.G., Pedlar A., 1993, *ApJ*, 419, 553
- Boksenberg et al., 1995, *ApJ*, 440, 151
- Condon J.J., Anderson E., Broderick J.J., *AJ*, 109, 2318
- Dahari O.A. & De Robertis M.M., 1988, *ApJ*, 331, 727
- Evans I.N., Tsvetanov Z., Kriss G.A., Ford H.C., Caganoff S., Koratkar A.P., 1993, *ApJ*, 417, 82
- Haniff C.A., Wilson A.S., Ward M.J., 1988, *ApJ*, 334, 104
- Khachikian E.Y. & Weedman D.W., 1971, *Afz*, 7, 389
- Kukula M.J., Pedlar A., Baum S.A., O'Dea C.P., 1995, *MNRAS*, 276, 1262
- Kukula M.J., Holloway A.J., Pedlar A., Meaburn J., Lopez J.A., Axon D.J., Schilizzi R.T., Baum S.A., *MNRAS*, in press
- Meaburn J., Blundell B., Carling R., Gregory D.F., Keir D., Wynne C.G., 1984, *MNRAS*, 210, 463
- Meaburn J., Whitehead M., Pedlar A., 1989, *MNRAS*, 241, 1P
- Mundell C.G., Holloway A.J., Pedlar A., Meaburn J., Kukula M.J., Axon D.J., 1995, 275, 67
- Mundell C.G., 1995, PhD Thesis, University of Manchester
- Nilson P., 1973, *Uppsala General Catalogue of Galaxies*, Uppsala Univ. Press.
- Paturel G., Fougue P., Bottinelli L., Gouguenheim L., 1989, *Catalogue of Principal Galaxies*, Observatoire de Lyon.
- Pedlar A., Meaburn J., Axon D.J., Unger S.W., Whittle D.M., Meurs E.J.A., Ward M.J., 1989, *MNRAS*, 238, 863
- Pedlar A., Kukula M., Longley D.P.T., Muxlow T.W.B., Axon D.J., Baum S., O'Dea C., Unger S.W., 1993, *MNRAS*, 263, 471
- Pogge R.W., 1989, *ApJ*, 345, 730
- Robinson A. et al., 1994, *A&A*, 291, 351
- Storchi-Bergman T., Wilson A.S., Baldwin J.A., 1992, *ApJ*, 396, 45
- Tadhunter C., Tsvetanov Z., 1989, *Nat*, 341, 422
- Taylor D., Dyson J.E., Axon D.J., 1992, *MNRAS*, 255, 351
- Tsvetanov Z.I., Kriss G.A. & Ford H.C., 1994, In "Proceedings of the Oxford Torus Workshop", ed. M.J. Ward, p63
- Ulvestad J.S., Wilson A.S., 1984, *ApJ*, 285, 439
- Unger S.W., Pedlar A., Axon D.J., Whittle M., Meurs E.J.A., Ward M.J., 1987, *MNRAS*, 228, 671
- Unger S.W., Lewis J.R., Pedlar A., Axon D.J., 1992, *MNRAS*, 258, 371
- Veilleux, S., 1991, *ApJ*, 369, 331
- Veron-Cetty M.P., Veron P., 1985, *A Catalogue of Quasars and Active Nuclei* (2nd ed.), ESO Sci. Rept no.4
- Whittle D.M., Haniff C., Ward M.J., Meurs E.J.A., Pedlar A., Unger S.W., Axon D.J., Harrison B., 1986, *MNRAS*, 222, 189
- Wilson A.S., Tsvetanov Z., 1994, *ApJ*, 107, 1227
- Wilson A.S., Ulvestad J.S., 1987, *ApJ*, 319, 105